0180

AN ANALYTICAL METHOD FOR VERTICAL BEHAVIOR OF SLIP LAYER PILE DURING AN EARTHQUAKE

Ting XU[1], Koji TOMINAGA[2] And Haruyuki YAMAMOTO[3]

SUMMARY

A series of shearing tests were performed on B grade asphaltic bitumen, which is the typical material for the slip layer to reduce the negative skin friction acting on end-bearing-piles embedded in consolidating soil. The experimental results show that the slip layer material is sensitive to shear strain speed and that the skeleton curve of the shearing stress-strain relationship is dependent on the shear strain speed. Based on the results, we present a mathematical model of the stress-strain relations for the slip layer under cyclic shearing, and carried out some parametric analysis for the pile-slip layer-soil system, where the pile head is vertically loaded with cyclic forces caused by seismic rocking generally. Analysis results show that the cyclic resistance at the pile head is generally larger in clay than in sand; the longer period of the rocking makes the resistance less at the pile head; the phenomena mentioned above are conspicuous only for the soil having great strength; and the head resistance of the SL pile is less than of an ordinary pile, but the gap is not large.

INTRODUCTION

When end-bearing piles are adopted to make a foundation on reclamation soil, the negative skin friction (NF) acting on pile, which happens accompanying with the ground subsidence, must be considered in foundation design. One method of reducing the negative friction force is to apply some slip layer (SL) on pile surface. The slip layer can be regarded as elastic material when suffered a rapid shear deformation, and as viscous liquid under slow but steady shear loading just like the NF force. The B grade asphaltic bitumen, a kind of special asphalt developed by Shell in the Netherlands, is such a material, and usually used to coat piles to reduce negative friction.

In respect to research on SL material for investigating its reduction effort of NF when an end-bearing-pile is embedded in consolidating soil, Bjerrum etc. (1969), Walker etc. (1973) and Clossen etc. (1974) with their comparison tests on special asphalt coated piles and uncoated piles can be regarded as pioneers. Later, the model tests by Shibata etc. (1982) and element tests on SL material shearing characteristics by Nakazawa and Yamagata (1984) are also observed.

Actually, when SL piles are suffered seismic loading, the SL material will endure speedy shear deformation. Research concerning such conditions is rarely seen. This paper shows a series of element tests on shearing properties of B grade asphaltic bitumen under different shear strain speeds and cyclic shearing load. Based upon the experiment results, the relationship of stress and strain was modeling, and still more, a set of parametric numerical analysis were executed for the pile-slip layer-soil system, where the pile head is loaded with cyclic vertical displacement caused by seismic rocking.

[1] *Hiroshima University Kagamiyama 1-5-1, Higashi-Hiroshima City, Japan ting@ipc.hiroshima-u.ac.jp*
[2] *Hiroshima University Kagamiyama 1-5-1, Higashi-Hiroshima City, Japan tomi@ipc.hiroshima-u.ac.jp*
[3] *Hiroshima University Kagamiyama 1-5-1, Higashi-Hiroshima City, Japan yamamoto@idec.hiroshima-u.ac.jp*

SHEARING TESTON SLIP LAYER MATERIAL

Equipment for Test

Shearing tests were carried out with the equipment shown in Figure 1 developed for this research, which contains a set of loading unit and a constant temperature water tank. Specimen was made of SL material of B grade asphaltic bitumen, size 60mm(height) x 60mm(width) x 10mm(thickness). Two pieces of specimen were heated and pressed on both sides of a movable plate with no air remained in the adhesion surface, and fixed the opposite sides of the specimen to two external plates in the same way. Two-sided shearing test is realized by traveling the movable plate up and down relatively to the unmovable external plates.

As the SL material is very sensitive to temperature, the change of surrounding temperature will influence its deformation property greatly. For this reason, the specimen were merged into a constant temperature water tank when tests, in which a high accuracy thermal sensor and a set of water circulating device were working to control the temperature strictly (accuracy: plus or minus 0.1 degrees centigrade). In our research, the temperature of 15 degrees centigrade was adopted which is the average temperature in ground measured in various parts of Japan.

Kind of Test

During the uni-directional shearing tests, the shear strain speed was created as 5, 10, 20, 30, 40 and 50 %/sec separately, in which tests with constant shear strain speed and tests in which shear strain speed changed abruptly were included. Also, some cyclic shear tests with different strain amplitudes and different shear strain speeds were done.

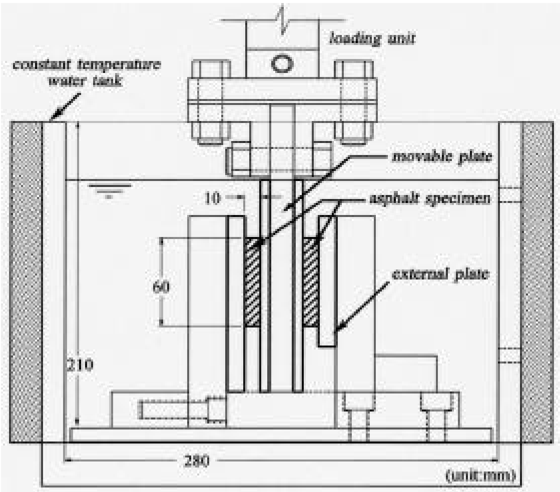

Figure 1: Equipment for test

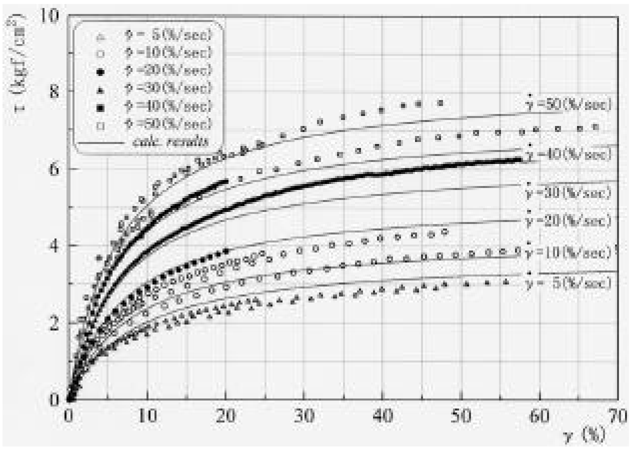

Figure 2: Shear stress ~ strain

MODELING

Shearing Stress-Strain Relationship

The results of simple shear tests, relationship of stress-strain, with different strain speeds are dotted in Figure 2. It can be found from the figure that the stress-strain relations are divided into several groups depending on the values of shear strain speed, because of their tendency appearing the same characteristics within one group.

To formulize the relationship of shear stress-strain of this SL material, we tried to make these curves approach to a hyperbolic function such as Equation 1

$$t = \frac{g}{Ag + B} \qquad (1)$$

where, the coefficients of *A* and *B* were evaluated by the least-squares method. In concrete, considering *1/A* and *1/B* as the convergent value of shear stress and initial grade separately, which depend on the strain speed, we fitted their relationship with strain speed to linear ones shown as Figure 3 and 4, formulized as Equation 2. From

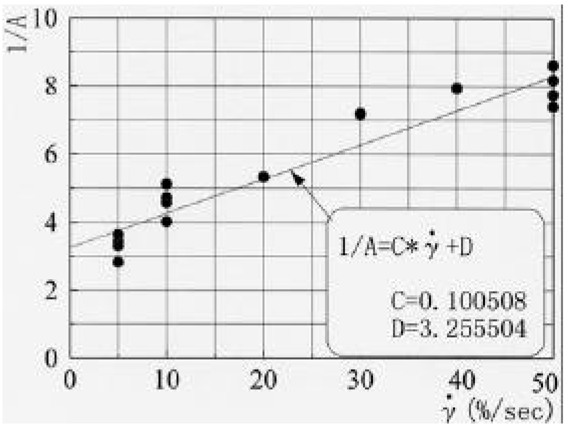

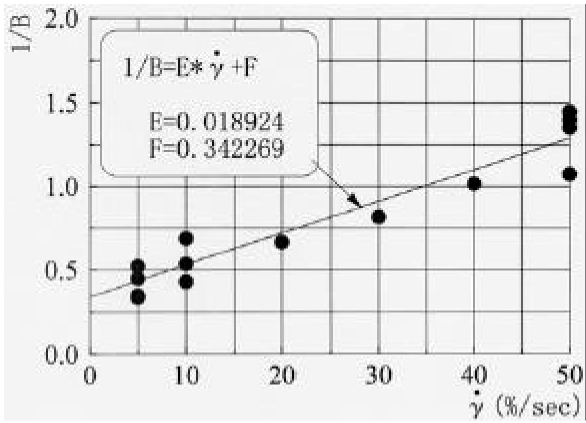

Figure 3: *1/A* ~ shear strain speed

Figure 4: *1/B* ~ shear strain speed

this modeling, we can grasp the meaning of group-divided more clearly, that is, the different values of shear strain speed divide the relationship curves into different groups. Solid curves in Figure 2 illustrate the calculating values of stress-strain relationship corresponding to different strain speeds.

$$\begin{cases} \dfrac{1}{A} = C\dot{\gamma} + D \\ \dfrac{1}{B} = E\dot{\gamma} + F \end{cases} \qquad (2)$$

The constants in Equation 2 were solved as *C*=0.100508, *D*=3.255504, *E*=0.018924 and *F*=0.342269.

Modified Masing's Law

Figure 5 shows the stress-strain relationship of the asphaltic bitumen obtained from the cyclic shear test with the strain amplitude of 10% and the shear strain speed of 10%/sec. Considering the spindle-shape of the stress-strain loops, the hysteretic curves are satisfying the Masing's Law with a coefficiet of 2 as indicated in Figure 6, that is,

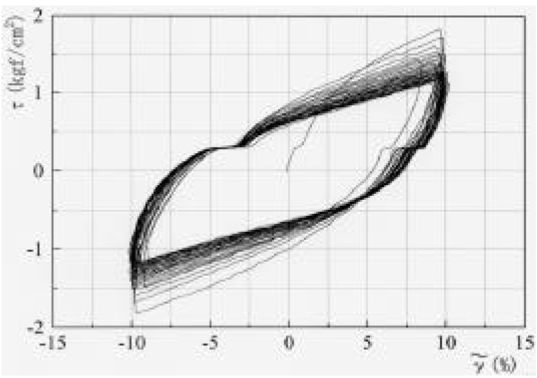

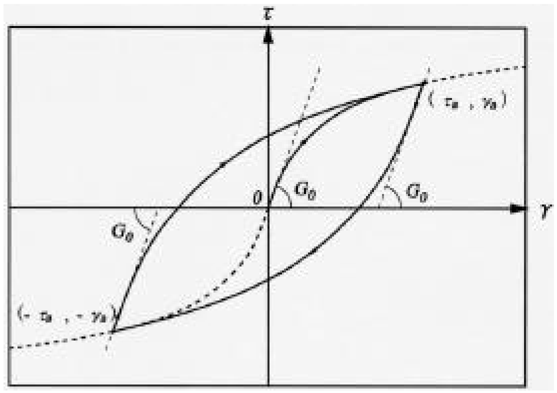

Figure 5: Result of a cyclic shearing test

Figure 6: Masing's law

the hysteretic curves can be expressed as Equation 3.

$$\frac{\tau - \tau_a}{2} = \frac{\dfrac{\gamma - \gamma_a}{2}}{A \cdot \dfrac{\gamma - \gamma_a}{2} + B} \qquad (3)$$

Where, (t_a, g_a) is the coordinates of a turning point.

Just as Equation 2 shows that both the skeleton and hysteretic curves are dependent on the shear strain speed when deformation occurs, the Masing's Law must be modified here to adapt to the situation. To understand the effect of the changing shear strain speed, we performed a series of shear tests, on the way of which shear strain speeds were changed suddenly. Figure 7 and 8 show the appearances of the strain speed changed from 40 to 20 and to 60%/sec respectively as example. It becomes clear from these experimental results that a stress-strain curve (skeleton curve) changes to another curve when its shear strain speed is changed, and these skeleton curves are determined by their strain speed separately. So, the Masing's Law was modified as shown in Figure 9, and the skeleton and hysteretic curves are expressed as Equation 4 and 5 when the shear strain speed is supposed as a constant during an increment.

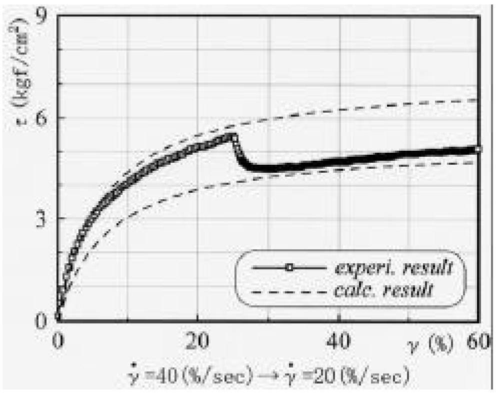

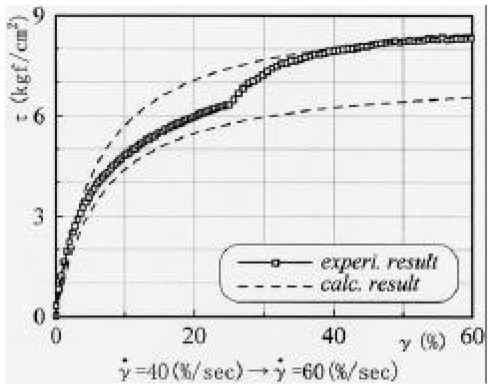

Figure 7: Reducing of strain speed

Figure 8: Elevating of strain speed

$$\begin{cases} \tau = \dfrac{\gamma}{A_m \gamma + B_m} \\ \dfrac{\tau - \tau_{am}}{2} = \dfrac{\dfrac{\gamma - \gamma_{ak}}{2}}{A_m \dfrac{\gamma - \gamma_{ak}}{2} + B_m} \end{cases} \tag{4}$$

$$\begin{cases} \dfrac{1}{A_m} = C\dot{\gamma}_{m-1} + D \\ \dfrac{1}{B_m} = E\dot{\gamma}_{m-1} + F \end{cases} \tag{5}$$

Where, A_m, B_m are the coefficients of the hyperbola when *m*th step, and $\dot{g}_{m-1}$ is the strain speed in *(m-1)*th step; (t_{am}, g_{ak}) is the coordinates of the turning point in *k*th curve and *m*th step.

In actual numerical calculating, the strain increment was set as very small one and the tangent grade in start point of a step was used as the shear stiffness of the asphalt.

NUMERICAL ANALYSIS

Analysis Model

In our research, the problem in which a cyclic axial force is applied on a SL pile head by superstructure rocking had been replaced with the problem of controlling pile head displacement, and the analysis of behavior of the SL pile is formulated based on the principle of virtual work. Figure 10 shows the model of numerical analysis for the system of pile-slip layer-soil. The pile itself was assumed to be an elastic body. The slip layer around the pile was expressed as SL interface elements, while the uncoated part of pile surface was expressed as slide elements of stiff-elastic type (dummy interface elements). Furthermore, slide elements of elastic-plastic type (ground interface elements) were disposed in the outer side, with whose boundary springs the friction between

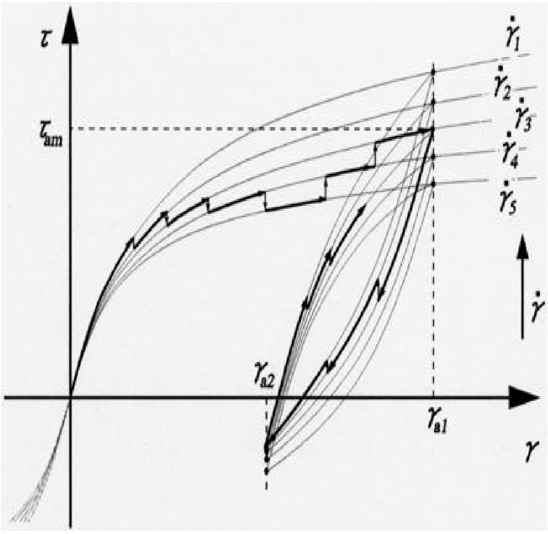

Figure 9: Modified Masing's law for slip layer

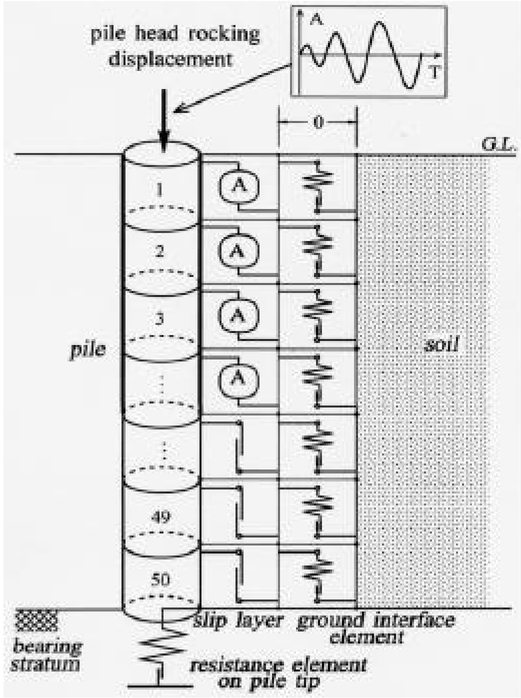

Figure 10: Numerical analysis model

SL pile and neighborhood ground was expressed. We also established a pile tip resistance element to express the penetration into bearing stratum.

Parameter

The parameters of steel pipe pile, slip layer and soil-pile interface are shown in Table 1. The pile and the B grade asphaltic slip layer are used actually in some foundation projects. The low part of 10m of the pile is not coated by slip layer. For numerical calculating, each of them is divided as 50 discrete elements along the depth of 50m. Because the stiffness and strength of soil are predicted to have influence on the effect of slip layer, cohesive and sandy soil, 3 kinds of strength values shown in Figure 11, in total, 6 cases of ground were adopted in analyses. As forced input wave acting on pile head vertically, the rocking displacement was design as sine and triangular waves shown in Figure 12, the former is a speed changing wave and the later a speed constant one. The period of waves was applied separately as 0.1, 1.0 and 10.0sec. Consequently, the shear strain speed of asphaltic slip layer, corresponding to rocking displacement speed of SL pile, is determined by the amplitude and period of the input wave. Table 2 shows the 28 executed cases of parametric analysis, comparing the results of which we examined the effect of parameters on behavior of the SL pile.

Table 1: Constants for analysis

Pile	Length (H) Diameter (D) Thickness of pile wall (t) Area of pile tip (A_{pc}) Modulus of elasticity (E_p)	50.0(m) 100(m) 1.6(cm) 7850(cm^2) 2.1×10^6(kgf/cm^2)
Slip layer	Coated thickness (d) Coated length (l)	0.6(cm) 40.0(m)
Ground	Limited relative displacement between pile and ground (U_{lim}) Limited friction stress (f_u)	1.0(cm) 0.5~20.0(kgf/cm^2)
Resistance element in pile tip	Maximum supporting stress (σ_{pmax}) Stiffness of spring (K_p)	100.0(kgf/cm^2) 75.0(kgf/cm^3)

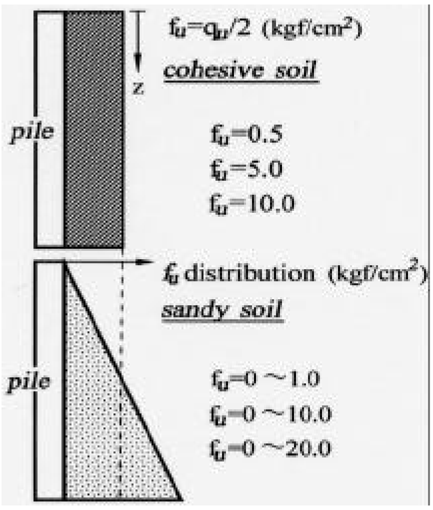

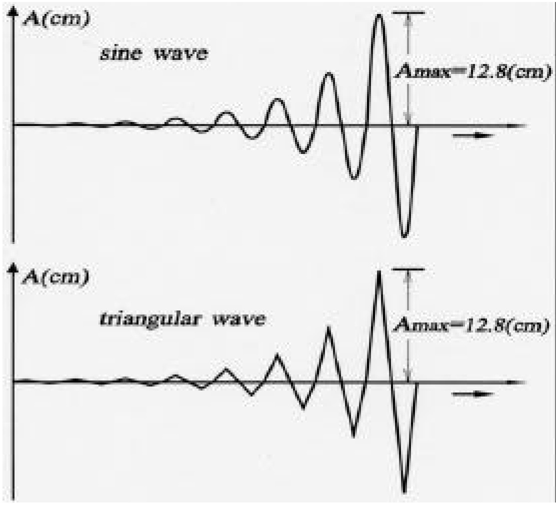

Figure 11: Soil conditions adopted in analysis **Figure 12: Input displacement wave on pile head**

Table 2: Parameters of analysis (1~28: number of case)

		Sine Wave			Triangular Wave		
		T=0.1	T=1	T=10	T=0.1	T=1	T=10
Clay	f_u=0.5		1	2		3	4
	f_u=5	5	6	7		8	9
	f_u=10	10	11	12		13	14
Sand	f_u=0~1		15	16		17	18
	f_u=0~10	19	20	21		22	23
	f_u=0~20	24	25	26		27	28

Result and Discussion

To compare the analytical results for sandy soil with cohesive soil, Figure 13 shows the relationship of reacting force on pile head P and pile head displacement U of the SL pile in cases of No.6, 7, 20 and 21. As shown in this figure, larger reacting force appears generally in case of cohesive soil.

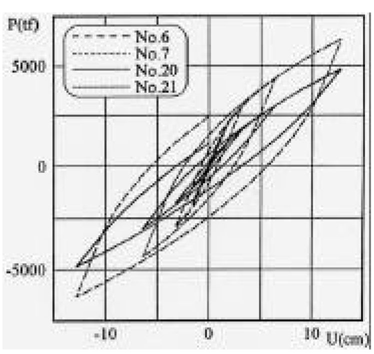

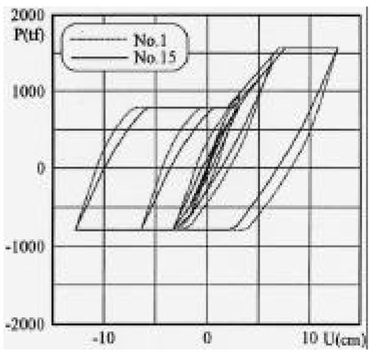

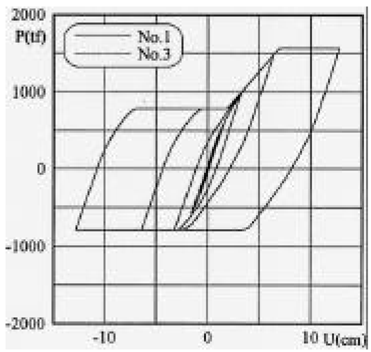

Figure 13: P~U (No.6, 7, 20 and 21) Figure 14: P~U (No.1 and 15) Figure 15: P~U (No.1 and 3)

While in Figure 14, we find in case of No.1 and 15, both of them are in soil condition of weak strength, there is no clear difference of the peak values of reacting force on pile head. The reason for this phenomenon is that when pile head displacement exceeds a specific value, either in case of cohesive or sandy soil, all of the ground interface elements in the system will turn into plastic condition, then the reacting forces on pile head here will reach a same limit value.

Similar situations can be seen in Figure 15 and 16 where the effect of the type (sine or triangular) and the period of input waves were investigated. The reason is as the same mentioned above. But in strong strength soil condition, consequences were some different. As shown in Figure 17 and 18, when in the condition of long period (T=10.0sec) the sine wave resulted in larger peak value of reacting force on pile head than triangular input; and input wave with a shorter period (higher speed) led to larger peak of the reacting force.

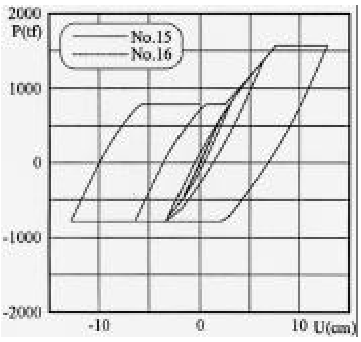

Figure 16: P~U (No.15 and 16)

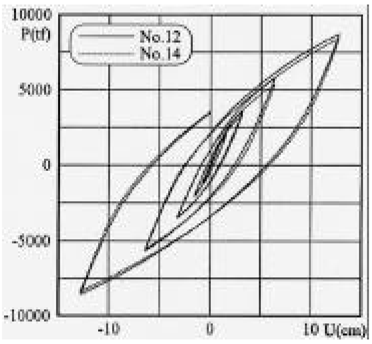

Figure 17: P~U (No.12 and 14)

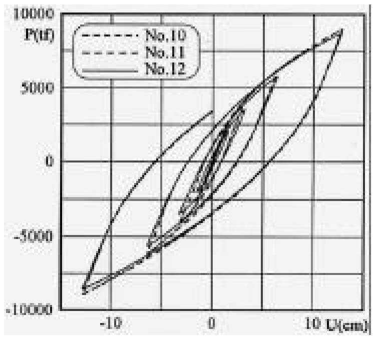

Figure 18: P~U (No.10, 11 and 12)

We also performed some numerical analyses with same parameters to compare ordinary pile (no slip layer coated) with SL pile. The ordinary pile displayed a larger head resistance than SL piles, but the difference was small.

CONCLUSION

It should be concluded, from what has been discussed above, that the slip layer material is highly sensitive to shear strain speed. The skeleton curve of the shear stress-strain relationship can be looked as a monotone increasing function of the shear strain speed, and the faster the strain speed is, the larger the shearing resistance appears. When the strain speed is changed suddenly in the way of shearing test, the stress-strain relationship curve will converge to the skeleton curve corresponding to the changed speed firmly. The cyclic resistance at the SL pile head is generally larger in clay than in sand. The longer period of the rocking makes the resistance less at the pile head. The appearances of SL pile mentioned above are conspicuous only for the soil having great strength. And, although the head resistance of the SL pile is less than of an ordinary pile, the gap is not large.

ACKNOWLEDGMENT

Thanks are due to Mr. S. Harada of Hiroshima University, graduate students of same university, H. Hamada (now working in Kumagai Corporation) and K. Kobayashi (now working in Asanuma Corporation) for their assistance in the research.

REFERENCE

Bjerrum. L, Johannessen and I. J. Eido. O (1969), "Reduction of Negative Skin Friction on Steel Piles to Rock", *Proc. 7th I.C.S.M.F.E.*, 2, pp27-34

Clossen, A. I. M. and Horvat, E. (1974), "Reducing Negative Friction with Bitumen Slip Layers", *Journal of ASCE*, 100, GT8, pp925-944

Nakazawa, Y. and Yamagata, K. (1986), "Stiffness Modulus of Bitumen on the Vertical Loading Tests of SL Piles", *Journal of Structural and Construction Engineering (Transactions of AIJ)*, 368, pp49-56

Shibata, T., Sekigutchi, H. and Yukitomo, H. (1982), "Model Test and Analysis of Negative Friction Acting on Pile", *Soil and Foundation*, 22, 2, pp29-39

Walker, L. K. and Darvall, P. LE. P. (1973), "Dragdown on Coated and Uncoated Piles", *Proc. 8th I.C.S.M.F.E.*, 2, pp257-262